Multistep Binding of Transition Metals to the H−N−H Endonuclease Toxin Colicin E9[†]

Anthony H. Keeble,[‡,⊥] Andrew M. Hemmings,[‡,§] Richard James,[#] Geoffrey R. Moore,[§] and Colin Kleanthous*[,‡,⊥]

School of Biological Sciences, University of East Anglia, Norwich NR4 7TJ, United Kingdom, School of Chemical Sciences, University of East Anglia, Norwich NR4 7TJ, United Kingdom, and Division of Microbiology & Infectious Diseases, University Hospital, Queen's Medical Centre, University of Nottingham, Nottingham NG7 2UH, United Kingdom

Received February 28, 2002; Revised Manuscript Received May 3, 2002

ABSTRACT: We report the first stopped-flow fluorescence analysis of transition metal binding (Co^{2+}, Ni^{2+}, Cu^{2+}, and Zn^{2+}) to the H−N−H endonuclease motif within colicin E9 (the E9 DNase). The H−N−H consensus forms the active site core of a number of endonuclease groups but is also structurally homologous to the so-called treble-clef motif, a ubiquitous zinc-binding motif found in a wide variety of metalloproteins. We find that all the transition metal ions tested bind via multistep mechanisms. Binding was further dissected for Ni^{2+} and Zn^{2+} ions through the use of E9 DNase single tryptophan mutants, which demonstrated that most steps reflect conformational rearrangements that occur after the bimolecular collision, many common to the two metals, while one appears specific to zinc. The kinetically derived equilibrium dissociation constants (K_d) for transition metal binding to the E9 DNase agree with previously determined equilibrium measurements and so confirm the validity of the derived kinetic mechanisms. Zn^{2+} binds tightest to the enzyme ($K_d \sim 10^{-9}$ M) but does not support endonuclease activity, whereas the other metals ($K_d \sim 10^{-6}$ M) are active in endonuclease assays implying that the additional step seen for Zn^{2+} traps the enzyme in an inactive but high affinity state. Metal-induced conformational changes are likely to be a conserved feature of H−N−H/treble clef motif proteins since similar Zn^{2+}-induced, multistep binding was observed for other colicin DNases. Moreover, they appear to be independent both of the conformational heterogeneity that is naturally present within the E9 DNase at equilibrium, as well as the conformational changes that accompany the binding of its cognate inhibitor protein Im9.

The human genome encodes an abundance of transition metal binding proteins, many of which are zinc-fingers (*1*). Although many Zn^{2+} binding proteins have been structurally characterized and the thermodynamic stability of metal binding determined, comparatively few studies have examined the mechanism of transition metal binding to such proteins. In the present study, we analyze the binding mechanism of Zn^{2+} and other first row transition metals to the H−N−H motif of colicin endonucleases (DNases), a metal binding motif found in prokaryotic and eukaryotic proteins.

Colicins are a group of protein antibiotics produced by, and active against, strains of *Escherichia coli* (*2*). The proposed active site cleft for the DNase domain of colicin E9 (E9 DNase[1]), in common with the other DNase type colicins, contains the consensus sequence for a group of intron-encoded endonucleases called H−N−H endonucleases (*3*, *4*). Intron and intein-encoded endonucleases, found in all three biological kingdoms, promote the homing of the genes encoding them by site-specifically cleaving intronless or inteinless alleles (*5*, *6*). As well as being common among homing enzymes, the H−N−H motif has also been identified in a number of other endonucleases (*7*), as well as in mismatch repair enzymes (*8*), recombinases (*9*), and type IIS restriction endonucleases (*10*). In contrast to highly specific enzymes such as the homing endonucleases, the H−N−H motif of the cytotoxic colicin DNases is used to cleave chromosomal DNA randomly, albeit with a preference for cleaving at T's (*11*).

At present, the only published crystal structures of H−N−H endonucleases are those of the 15 kDa DNase domains of colicins E9 (*12*) and E7 (*13*), with both enzymes shown to bind transition metals within the H−N−H motif, nickel in the case of E9 (*12*) and zinc in E7 (*13*). The H−N−H motif comprises a $\beta\beta\alpha$ zinc fingerlike fold with metal ligating histidine residues originating from the secondary structural elements. In the crystal structures of E9 and

[†] This research was supported by the Wellcome Trust. A.H.K. was supported by a Wellcome Trust Prize Studentship.

* To whom correspondence should be addressed. Tel: +44 (0)1904 328820. E-mail: ck11@york.ac.uk.

[‡] School of Biological Sciences, University of East Anglia.

[§] School of Chemical Sciences, University of East Anglia.

[#] University of Nottingham.

[⊥] Present address: Department of Biology, University of York, Heslington York Y010 5DD, U.K.

[1] Abbreviations: E9 DNase, endonuclease domain of colicin E9; Im9, immunity protein for colicin E9 DNase; k_{obsn}, observed rate constant for the *n*th step; ΔF_{total}, total observed change in fluorescence; ΔF_{kobsn}, fluorescence amplitude associated with observed rate constant; $k_n + k_{-n}$, the derived rate constants for the *n*th step; ANS, 8-anilinonaphthalenesulfonic acid; W22+, a tryptophan-to-phenylalanine mutant of the E9 DNase (W58F) that contains only Trp22; W58+, a tryptophan-to-phenylalanine mutant of the E9 DNase (W22F) containing only Trp58; EDTA, ethylenediaminetetraacetic acid; HEPES, 4-(2-hydroxythyl)-piperazine-1-ethanesulfonic acid.

10.1021/bi020174o CCC: $22.00 © 2002 American Chemical Society
Published on Web 07/19/2002

E7 DNases, the coordination geometry of the bound metal ions conform to an approximate tetrahedron, with two or three protein ligands, and further ligands provided by phosphate or water in E9 and E7, respectively (*12*, *13*). In the case of the E9 DNase, crystallography identifies only two histidine ligands to the Ni^{2+}, with a third histidine in close proximity, while solution NMR studies indicate that three histidine residues are associated with the bound Ni^{2+} ion (*14*). The H−N−H motif is known to be the core of the colicin DNase active site since mutants within it abolish enzymatic activity (*15*). Moreover, the active sites of a number of other endonucleases such as the intron-encoded endonuclease I-*PpoI* from *Physarum polycephalum*, the nuclease from *Serratia marcescens*, and endo VII from phage T4 are structurally homologous to the active site of colicin DNases. Intriguingly, a transition metal-binding histidine residue within the motif is the functional equivalent of a Mg^{2+}-binding asparagine in both I-*PpoI* and *Serratia* nuclease (*16*). Furthermore, the protein fold around the metal site in colicin DNases is conserved among a much larger group of proteins called treble-clef zinc-finger motif proteins (*17*). This group of proteins binds Zn^{2+} in a predominately structural role, and includes ribosomal proteins as well as proteins involved in cell signaling and endosome fusion events. The structural similarity of some of these proteins to classical zinc finger proteins has also previously been noted (*18*).

The E9 DNase H−N−H motif is a good model with which to investigate the kinetic mechanism of transition metal binding to a ubiquitous metal binding motif since there is high-resolution structural information and thermodynamic data for protein−metal complexes (*12*, *19*, *20*). In the present study, we use stopped-flow spectrofluorimetry to investigate the rates and mechanisms of binding of Co^{2+}, Ni^{2+}, Cu^{2+}, and Zn^{2+} to the E9 DNase. We find that each metal binds through a multistep mechanism reflecting conformational changes in the H−N−H motif, and these are discussed in the context of thermodynamic data (*20*), their relationship to other conformational changes experienced by the E9 DNase (*21*, *22*), their ability to support DNase activity (*11*, *20*, *23*), and structural information on DNase−metal complexes (*12*, *19*).

To express their cytotoxic activities, endonuclease colicins must first bind to a target bacterial cell and then translocate across the outer membrane, periplasm, and finally the inner membrane. Entry is gained by parasitization of nutrient uptake proteins (*24*). E group DNase colicins are released as a heterodimeric complex with a small (∼9.5 kDa) soluble protein, called an immunity protein, that binds and inactivates the DNase domain of the colicin with very high affinity ($K_d \sim 10^{-14}$ M), thereby preventing the suicide of the producing cell (*25*, *26*). Hence, for a DNase colicin to present its cytotoxic activity the immunity protein must dissociate during translocation. However, it has been noted that colicin E9 freed of its endogenous immunity protein Im9 shows the same rate of cell killing as the heterodimeric complex implying that Im9 dissociation is not rate-limiting for cell death. Yet, the in vitro dissociation rate constant for the E9 DNase−Im9 complex (10^{-6} s^{-1}) is far slower than the rate of cell death at 37 °C ($\sim 10^{-3}$ s^{-1}) (*22*). To resolve this paradox, we proposed previously that through the structural stabilization induced by transition metal binding (the melting point of the protein increases by 22 °C), the loss of metal from the H−N−H motif could destabilize the colicin E9−immunity protein complex sufficiently to accelerate dissociation of the complex (*20*). This hypothesis was tested in the present study by determining the association and dissociation kinetics of immunity protein Im9 binding the E9 DNase in vitro in the presence and absence of bound zinc.

MATERIALS AND METHODS

Materials. Buffers, media, and metal ion dichlorides were purchased from Sigma or BDH-Merck. Metal ion solutions were freshly prepared for each experiment.

Bacterial Strains and Media. Plasmid pRJ353 (encoding the E9 DNase domain and Im9 with a C-terminal histidine tag) was transformed into *Escherichia coli* BL21 (DE3) pLysS and cells were grown on Luria-Bertani broth, essentially as described previously (*15*).

Site-Directed Mutagenesis. Engineering individual tryptophan-to-phenylalanine mutants generated E9 DNases containing a single tryptophan, W22+ (which contained the W58F mutation) and W58+ (which contained the W22F mutation), respectively. PCR mutagenesis of plasmid pRJ353 containing the E9 DNase and Im9 proteins in a single operon was carried out using standard protocols. HPLC purified primers were supplied by MWG-Biotech. Presence of the mutation was confirmed by DNA sequencing and electrospray ionization mass spectrometry of the purified proteins.

Protein Purification and Protein Determinations. Wild-type and single-tryptophan variants of the E9 DNase, as well as the E2, E7, and E8 DNases were purified as described previously (*15*) with the modification that after elution of the protein, metals were removed by treatment with EDTA followed by extensive dialysis against high salt buffers before lyophilization from water (*20*). The dithiol containing E9 DNase (E9 DNase D20C/E66C double mutant) was purified and prepared in the oxidized and reduced states as described previously (*27*). Im9 was purified as described by Wallis et al. (*22*). DNase domains and immunity proteins were quantified by absorbance spectrophotometry and confirmed to be metal free using previously described methods (*20*, *22*). Amino acid analysis of the single tryptophan variants was performed (Alta Biosciences, Birmingham, UK) to determine their altered extinction coefficients (10 700 M^{-1} cm^{-1}).

Stopped-Flow Spectrofluorimetry. Experiments were performed at 25 °C with an SX-18MV stopped-flow spectrofluorimeter (Applied Photophysics Ltd, Leatherhead, U.K.) in 1:1 mixing mode using a single monochromator with a 9-nm bandwidth and an excitation wavelength of 295 nm to eliminate photobleaching (trace of E9 DNase mixed against buffer was flat). All fluorescence data were collected above 305 nm using a cutoff filter to monitor intrinsic tryptophan fluorescence. To improve data analysis in cases where multiple transients were observed over a range of time-scales, the data were collected using a log time base to ensure an equal number of data points over each time division (*28*). All concentrations quoted refer to those present in the reaction cell.

Metal Association Kinetics. The final concentration of E9 DNase used (unless stated otherwise) was 16.5 μM, which ensured a good signal-to-noise ratio and that the different

fluorescence decay phases were well separated while minimizing inner filter effects. The buffer used for the standard assay was 50 mM triethanolamine, pH 7.5. In all cases, 1 mM stock solutions of the metal were prepared in the appropriate buffer and diluted into the same buffer minus metal as required. Ten runs were averaged for each rate, and the first 0.002 s were ignored for fitting purposes. Under pseudo-first-order conditions, kinetic traces were analyzed by fitting differing numbers of exponentials (eqs 1−4) as appropriate:

$$F = \Delta F \exp(-k_{obs1}t) + F_e \quad (1)$$

$$F = \Delta F_1 \exp(-k_{obs1}t) + \Delta F_2 \exp(-k_{obs2}t) + F_e \quad (2)$$

$$F = \Delta F_1 \exp(-k_{obs1}t) + \Delta F_2 \exp(-k_{obs2}t) + \Delta F_3 \exp(-k_{obs3}t) + F_e \quad (3)$$

$$F = \Delta F_1 \exp(-k_{obs1}t) + \Delta F_2 \exp(-k_{obs2}t) + \Delta F_3 \exp(-k_{obs3}t) + \Delta F_4 \exp(-k_{obs4}t) + F_e \quad (4)$$

where F is the fluorescence at time t, ΔF_n is the fluorescence change for the nth phase, k_{obsn} is the observed rate constant for the nth phase, and F_e is the end point fluorescence, by nonlinear regression using the Workstation software (Applied Photophysics Ltd) and Kaleidagraph (Synergy Software). Under second-order conditions, kinetic traces were fitted to eq 5,

$$F = F_0 + \Delta F_1 [N]_0 k_1 t/(1 + [N]_0 k_1 t) + \Delta F_2 \exp(-k_{obs2}t) + \Delta F_3 \exp(-k_{obs3}t) \quad (5)$$

where $[N_0]$ is the initial concentration of the E9 DNase and metal ion, and F_0 is the initial fluorescence. In eqs 1−5, the rate constants obtained by nonlinear regression are referred to as observed (or macroscopic) first-order rate constants to differentiate them from the derived microscopic rate constants (for example, the bimolecular rate constant k_1 in eq 5). Microscopic rate constants, k, were generally determined by the concentration dependence of observed rate constants, k_{obs}.

Association between the E9 DNase and the metal was normally carried out under pseudo-first-order conditions. Where k_{obs1} has a linear concentration dependence, as seen in the Co^{2+}, Cu^{2+}, and Zn^{2+} experiments, the bimolecular association rate was obtained by fitting the rate constants to eq 6,

$$k_{obs1} = k_1[\text{metal}] + k_{-1} \quad (6)$$

where k_{obs1} is the pseudo-first-order rate constant, k_1 is the bimolecular rate constant for E9 DNase-metal association, [metal] is the initial concentration of the metal, and k_{-1} is the dissociation rate constant of the metal from the encounter complex. In all cases, the R^2 value for the bimolecular rate was > 0.98. In the case of a two-step binding mechanism, for example, eq 6 holds true where $k_1[\text{metal}] + k_{-1} \gg k_2 + k_{-2}$, and so $k_{obs1} = k_1[\text{metal}] + k_{-1}$ and $k_{obs2} = k_2 + k_{-2}$. This is often the case for ligands that bind with a bimolecular rate constant close to the diffusion-controlled limit (10^7−10^9 M^{-1} s^{-1}) (*29*). However, when the bimolecular rate constant falls substantially below the diffusion controlled limit, it can become slow enough so that at the concentrations of ligand used, $k_2 + k_{-2} \gg k_1[\text{metal}] + k_{-1}$, where instead eqs 7 and 8 hold true,

Scheme 1

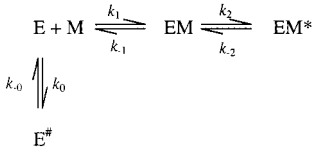

$$k_{obs1} = k_2 + k_{-2} \quad (7)$$

$$k_{obs2} = k_1[\text{metal}] + \text{constant} \quad (8)$$

In this case, k_{obs1} is concentration-independent and k_{obs2} has a linear concentration dependence with the gradient = k_1, and the intercept a constant obtained from $(k_{-1}k_{-2})/(k_2 + k_{-2})$ in the case of a two-step mechanism (*29*). Assuming rate coupling has a negligible effect (k_{obs1}, $k_{obs2} \gg k_{obs3}$), the general forms of eqs 7 and 8 should also hold true for analysis of a mechanism containing three steps. This form of analysis was applied to Ni^{2+} binding the E9 DNase.

Metal Dissociation Kinetics. Dissociation rate constants were determined by EDTA sequestration, a technique commonly used to investigate the kinetics of transition-metal dissociation from metalloproteins such as FosA (*30*) and carbonic anhydrase (*31*). The buffers used were the same as those for association kinetics. A slight excess of metal was preincubated with the E9 DNase (final concentration 13.2 μM) in the presence of 8-anilinonaphthalenesulfonic acid (20 μM; ANS) and rapidly mixed with 20 μM EDTA in the stopped-flow spectrofluorimeter. The EDTA-transition metal equilibrium constants are pM or tighter for all the metals tested and so the competing EDTA sequesters any dissociated metal ion (*32*). An excitation wavelength of 355 nm was used and ANS fluorescence monitored collecting all fluorescence above 455 nm using a cutoff filter with 5−10 runs averaged in each experiment. The resulting fluorescence enhancements were analyzed by fitting exponential equations as described above. Under these conditions, the binding of ANS to metal free protein was found to occur in the dead-time of the machine (data not shown).

Immunity Protein Binding Kinetics. These were carried out essentially as described by Wallis et al. (*22*) with apo- or zinc-bound E9 DNase.

Ligand Binding Mechanisms. Scheme 1 shows a comparison of the two general mechanisms for multistep binding for an enzyme (E) and its ligand (M) that form a 1:1 complex (assuming the conditions for eq 6 hold true).

When a conformational change is present in a mechanism, it can occur either *before* the bimolecular step (the vertical branch in Scheme 1) with the enzyme in equilibrium between an unreactive ($E^{\#}$) conformer and a reactive conformer (E) that can bind the ligand, or *after* it (the horizontal branch in Scheme 1) where an initial complex is formed (EM) that undergoes a conformational change to produce the final complex (EM*). In the simplest scenario of a two-step mechanism in which both steps are observed directly, the first step represents the bimolecular collision and the second step the conformational change. While both mechanisms predict that k_{obs1} should be linear with ligand concentration, they can be distinguished by the predicted concentration

dependence of k_{obs2}. When the conformational change occurs before ligand binding, eq 9 predicts that k_{obs2} should *decrease* from $k_0 + k_{-0}$ to k_{-0} as the concentration of the ligand, *M*, is increased.

$$k_{obs2} = k_{-0} + \left(\frac{k_0}{1 + ([M]/(K_{-1} + [E]))}\right) \quad (9)$$

where K_{-1} is the equilibrium constant (k_{-1}/k_1) for the binding step. In contrast, when the conformational change occurs after ligand binding, eq 10 predicts that k_{obs2} should *increase* from k_{-2} to $k_2 + k_{-2}$ (*33*).

$$k_{obs2} = \left(\frac{k_2}{1 + (K_{-1}/[M])}\right) + k_{-2} \quad (10)$$

Although the direction of concentration dependence is different between eqs 9 and 10, they both predict a hyperbolic change in k_{obs2}, diagnostic that the step represents a conformational change (*34*).

RESULTS AND DISCUSSION

Metal Binding to the E9 DNase Occurs in Multiple Steps. One of the great anomalies of the H−N−H motif of the colicin E9 DNase is that while it resembles the zinc site of a metalloenzyme such as carbonic anhydrase, bound Zn^{2+} does not support hydrolysis of any nucleic acid substrate, whereas Co^{2+}, Ni^{2+}, and Cu^{2+} all support DNase activity (*11*, *20*, *23*; AHK, unpublished observations). This contrasts with recent observations by Ku et al (*35*) with the E7 DNase (identical to E9 within the H−N−H motif) which purport to show that zinc is active with this enzyme. We note that the E7 DNase used in the study of Ku et al (*35*) was engineered with an N-terminal histidine tag and was purified by nickel-affinity chromatography, with the purified protein subsequently treated with EDTA and dialyzed overnight to remove the chelating agent. The present work used E9 DNase that was also purified by nickel-affinity chromatography, but where the histidine tag was engineered onto the Im9 protein that was subsequently separated from the DNase by denaturation, treated with EDTA, and the DNase refolded (*20*). Importantly, we have shown previously that the E9 DNase (pI of 9.5) readily associates with Ni^{2+}-EDTA (*14*), the removal of which requires either extensive high salt dialysis (used in the present study) or gel-filtration under denaturing conditions (*20*). Protein prepared in this way binds transition metals stoichiometrically and is inactive with Zn^{2+} but active with Ni^{2+} ions. E7 DNase prepared in our laboratory using this procedure yields identical activity and equilibrium metal binding data to those of the E9 DNase (data not shown).

Transition metal binding to the E9 DNase results in a small quench (~10%) in the intrinsic tryptophan fluorescence of the protein (*20*), and so the kinetics of metal binding (Zn^{2+}, Co^{2+}, Ni^{2+}, and Cu^{2+}) were investigated using stopped-flow fluorescence. An example stopped-flow trace for Zn^{2+} binding is shown in Figure 1. Three exponential decays were observed over a range of time-scales from tens of milliseconds to minutes, suggesting that Zn^{2+} binding can be minimally described by a three-step mechanism. The total fluorescence change (ΔF_{total}) for Zn^{2+} binding, as with the other metals tested, was very close to that determined from

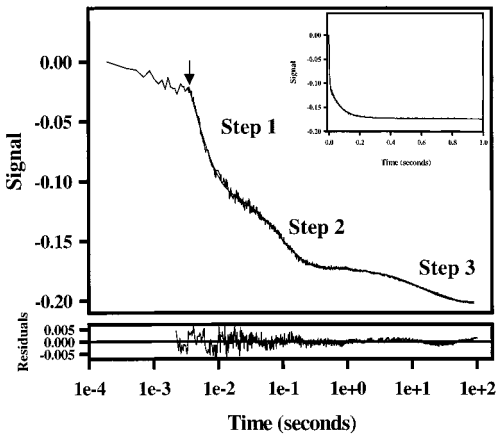

FIGURE 1: Stopped-flow tryptophan fluorescence data showing binding of 16.5 μM apo-E9 DNase to 165.5 μM Zn^{2+} in 50 mM triethanolamine, pH 7.5, and at 25 °C. The main figure is shown on a logarithmic time base and the three steps that minimally describe the process indicated. The data were collected with a small pre-trigger, with the data from 2 ms (indicated with an arrow) fitted to a triple exponential equation (see Materials and Methods) to produce $k_{obs1} = 255\ s^{-1}$ ($\Delta F_{kobs1} = 0.092$), which increases linearly with Zn^{2+} concentration, $k_{obs2} = 14\ s^{-1}$ ($\Delta F_{kobs2} = 0.071$), and $k_{obs3} = 0.07\ s^{-1}$ ($\Delta F_{kobs3} = 0.028$). The fit to the data is also shown. The Zn^{2+} concentration-dependence of k_{obs2} and ΔF_{kobs2} are presented in Figure 4. Inset, the first second of the stopped-flow data are shown on a linear time scale for comparison. Lower panel, residuals for the fit to the triple exponential equation.

static fluorimetric experiments, suggesting that there are no processes (which yield a fluorescence change) occurring in the dead-time of the instrument (~1.2−1.7 ms). Multistep binding kinetics, with the same number of steps, are seen with both HEPES (data not shown) and triethanolamine, the latter adopted in the present study to allow direct comparison with previous thermodynamic data (*20*). That similar effects are seen with different buffers also demonstrates that it is the binding of metal to the DNase that is rate-limiting rather than metal release from buffer.

Complex kinetics are also observed for Co^{2+}, Ni^{2+}, and Cu^{2+} binding (Figure 2) with Co^{2+} having two steps, and Ni^{2+} and Cu^{2+} each having three steps. Figure 2 illustrates that association of the different metal-chloride salts occurs over a wide range of rate constants, implying that it is the binding of the metal ion rather than the chloride ion being observed, and that each metal ion can have a quite different ΔF_{total}. Multistep binding of transition metals to proteins has been reported previously, particularly for Mn^{2+} binding to the Fosfomycin resistance protein (FosA) where a five step binding mechanism was proposed (*30*). These initial experiments do not suggest any simple correlation between transition-metal ion binding mechanism and metal ion-supported enzymatic activity. However, as addressed below, this does not discount the possibility that additional, spectroscopically silent, steps occur for Zn^{2+}-binding that are absent for the other metals.

Determination of the Bimolecular Rate Constants for Metal Binding. For Co^{2+}, Cu^{2+}, and Zn^{2+} binding, the plot of k_{obs1} against metal concentration was linear, implying that this process is monitoring the bimolecular step (see Materials and Methods). Therefore, the observed values for k_{obs1} for these metal ions were fitted to eq 6 to derive the bimolecular rate constant, k_1. The derived rate constants are summarized in Table 1 with Figure 3 showing representative data for

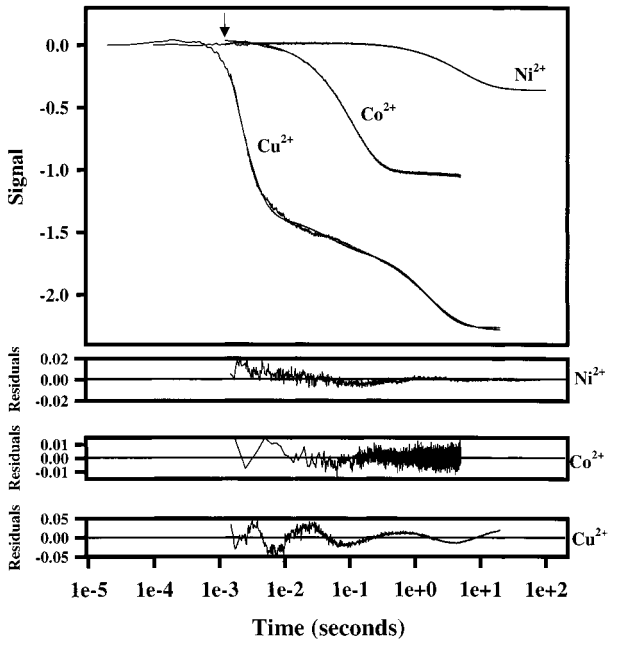

FIGURE 2: Stopped-flow tryptophan fluorescence traces for Cu^{2+}, Co^{2+}, and Ni^{2+} binding to apo-E9 DNase (top panel) showing the wide-range of time scales over which the different metals bind. All data were manually offset to start at zero signal for ease of comparison, and represent 16.5 μM E9 DNase binding metals under pseudo-first-order conditions (132.2 μM Cu^{2+} and Co^{2+}, and 198.6 μM Ni^{2+}) in 50 mM triethanolamine, pH 7.5, and at 25 °C. The Ni^{2+} data are shown fitted to a triple exponential equation to produce $k_{obs1} = 1.3\ s^{-1}$ ($\Delta F_{kobs1} = 0.09$), which is concentration-independent, $k_{obs2} = 0.195\ s^{-1}$ ($\Delta F_{kobs2} = 0.22$), which increases linearly with Ni^{2+} concentration, and $k_{obs3} = 0.074\ s^{-1}$ ($\Delta F_{kobs3} = 0.069$), which shows a complex concentration dependence (see Figure 4). The Co^{2+} data are shown fitted to a double exponential equation to produce $k_{obs1} = 9.07\ s^{-1}$ ($\Delta F_{kobs1} = 1.06$), which increases linearly with Co^{2+} concentration, and $k_{obs2} = 0.42\ s^{-1}$ ($\Delta F_{kobs2} = 0.044$), which is concentration independent. The Cu^{2+} data are shown fitted to a triple exponential equation to produce $k_{obs1} = 186.3\ s^{-1}$ ($\Delta F_{kobs1} = 1.19$), which increases linearly with Cu^{2+} concentration, $k_{obs2} = 21\ s^{-1}$ ($\Delta F_{kobs2} = 0.267$), and $k_{obs3} = 0.59\ s^{-1}$ ($\Delta F_{kobs3} = 0.649$), with both k_{obs2} and k_{obs3} being concentration-independent. The start of the fitted data (2 ms) is indicated with an arrow, with the fits overlaid on each data set. In contrast to Zn^{2+} binding, none of the observed rate processes have amplitude changes (ΔF) that are concentration dependent. Lower panels show residuals to the fitted equations. Although a pattern is observed in the residuals, this is small relative to the total amplitude change.

Zn^{2+} binding. For Zn^{2+}, Co^{2+}, and Cu^{2+}, the associated amplitude change, ΔF_{kobs1}, made the largest relative contribution by an individual step to ΔF_{total} (~95% for Co^{2+}, ~57% for Cu^{2+}, and ~48% for Zn^{2+}). In the case of Ni^{2+} binding, however, ΔF_{kobs2} made the largest relative contribution to ΔF_{total} (~58%) with k_{obs2} showing a linear concentration dependence and k_{obs1} being concentration-independent. In this instance, k_1 was derived by fitting the observed values of k_{obs2} to eq 8 (see Materials and Methods and Table 1) with k_{obs1} likely representing $k_2 + k_{-2}$.

The relative magnitudes of the bimolecular rate constants for Zn^{2+}, Co^{2+}, and Ni^{2+} parallel their respective water−ligand dissociation rates ($Zn^{2+} > Co^{2+} > Ni^{2+}$) (*36*), suggesting that this could play a role in determining the observed rate. However, the rates are an order of magnitude slower than expected, with the rate for Cu^{2+} retarded by 100-fold. Similar rate retardation is observed with Zn^{2+} binding to carbonic anhydrase (*31*, *37*). Rates below the water-exchange rate demonstrate that desolvation of the metal ion cannot be completely rate-limiting for association and imply that another undetected step is rate-limiting, such as a rapid protein conformational change or deprotonation(s) of a weak metal ion−water−protein complex (*30*).

Metal-Induced Conformational Changes. The E9 DNase is a monomeric protein that binds transition metals with a 1:1 stoichiometry (*20*, *23*). Therefore, the multistep binding kinetics likely reflect conformational changes either *before* or *after* the bimolecular step. The two possibilities can be distinguished by the distinct concentration dependence they each predict (see Materials and Methods and ref *33*). Both k_{obs2} and k_{obs3} for Zn^{2+} (Figure 4a for k_{obs2}) and k_{obs3} for Ni^{2+} (Figure 4b) are concentration-dependent, and initially the observed rate constants *increase* with metal ion concentration implying that the conformational changes occur after the bimolecular step. This is supported by the increase in the observed rate constants for the conformational change steps when the protein concentration was increased (data not shown), a situation that can only occur if the conformational change occurs after the bimolecular step (*38*). However, at higher metal ion concentrations the observed rate constants *decrease*, suggesting that the conformational change occurs before the bimolecular step. These apparently contradictory observations likely reflect further complexities in the metal binding mechanisms, such as the presence of spectroscopically silent steps (that perturbs the observed rate constants), or an inability to clearly resolve multiple transients (*39*), and are addressed below through the use of mutants.

The observed rate constants for the steps after the bimolecular step for Co^{2+} and Cu^{2+} binding were concentration-independent precluding further mechanistic analysis. It is likely, however, that they bind by a related mechanism to that for Zn^{2+} and Ni^{2+} given that they bind at the same site on the E9 DNase.

Metal-Induced Conformational Changes Occur Independently of Other Conformational Effects in the E9 DNase. Heteronuclear NMR experiments have demonstrated that the E9 DNase exhibits conformational heterogeneity in solution such that two distinct conformational states interconvert on the seconds time scale (*21*). Conformational changes within the E9 DNase have previously also been observed upon binding its cognate inhibitor, the immunity protein Im9 (*22*). Although these affect parts of the E9 DNase some distance from the metal site (Figure 5), it is nevertheless possible that the complex kinetics of metal ion binding are related to either of these processes, and so this was addressed in the following experiments. Mosbahi et al. (*27*) have demonstrated that an intramolecular disulfide bond engineered into the E9 DNase (the E9 DNase D20C/E66C double mutant) eliminates the intrinsic conformational heterogeneity of the enzyme and that this is regained when the disulfide is reduced. Multistep Zn^{2+} binding to this mutant was observed both in the presence and absence of the disulfide bond (Figure 6) suggesting that metal-induced conformational changes are distinct to those responsible for the conformational heterogeneity. This is also consistent with the observation that the presence of bound Zn^{2+} has little influence on the solution heterogeneity of the DNase detected by NMR (*40*).

To test whether the metal-induced conformational changes were related to those that occur upon Im9 binding, we

Table 1: Summary of the Derived Rate Constants for Transition Metal Binding to the E9 DNase in 50 mM Triethanolamine Buffer, pH 7.5, and at 25°C

rate constant	Co^{2+}	rel ΔF[a]	Ni^{2+}	rel ΔF	Cu^{2+}	rel ΔF	Zn^{2+}	rel ΔF[i]
k_1 (M^{-1} s^{-1})[b]	5.74×10^4	0.95	$1.55 (\pm 0.05) \times 10^3$	0.58[c]	1.24×10^6	0.57	$1.24 (\pm 0.01) \times 10^6$	0.48
k_{-1} (s^{-1})[d]	1.4		0.09 ($\pm$ 0.02)[d]		2		40 ($\pm$ 2)	
$k_2 + k_{-2}$ (s^{-1})[e]	0.5 ($\pm$ 0.1)	0.05	~2 ($\pm$ 0.3)	0.24	21 ($\pm$ 1)	0.13	~21	0.37
$k_3 + k_{-3}$ (s^{-1})[f]	n.d.	n.d.	0.07 ($\pm$ 0.01)	0.18	0.5 ($\pm$ 0.1)	0.31	0.07($\pm$ 0.01)	0.15
k_{off} (s^{-1})[g]	0.057 ($\pm$0.04)		~10^{-4} [h]		0.386 ($\pm$ 0.03)		0.0077 ($\pm$0.0003)	

[a] Relative fluorescence change. [b] Association rate constants were obtained by fitting the observed values for the observed rate constant that had a linear metal ion concentration dependence either to eq 6 for Co^{2+}, Cu^{2+}, and Zn^{2+} binding, where k_{obs1} was linear, or to eq 8 for Ni^{2+} binding where k_{obs2} was linear. [c] The associated amplitude change for the bimolecular step for Ni^{2+} binding was obtained from ΔF_{kobs2}. [d] Intercept from fitting k_{obs1} to eq 6 (Co^{2+}, Cu^{2+}, Zn^{2+}), or by fitting k_{obs2} to eq 8 (Ni^{2+}). [e] Plateaued (maximal) rate from the concentration dependence of k_{obs2} (Co^{2+}, Cu^{2+}, Zn^{2+}) or k_{obs1} (Ni^{2+}). [f] Plateaued (maximal) rate for the concentration dependence of k_{obs3} (Cu^{2+}, Ni^{2+}, Zn^{2+}). [g] k_{off} is the slowest observed rate for the dissociation of metal from the E9 DNase measured by EDTA capture. [h] The slowest dissociation phase for Ni^{2+} was too slow to measure accurately. [i] Relative ΔF for Zn^{2+} binding is concentration dependent, quoted values are for 165.5 μM Zn^{2+}. n.d., not detected.

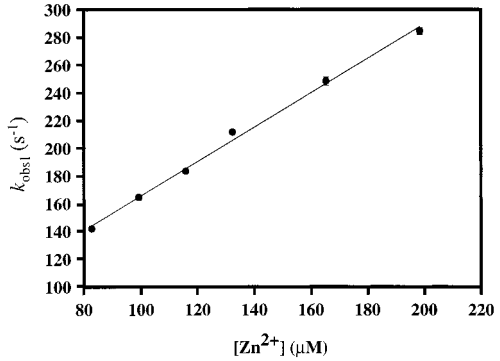

FIGURE 3: Concentration-dependence of the first transient (k_{obs1}) observed by stopped-flow fluorescence upon Zn^{2+} binding to the E9 DNase (see Figure 1). The data shown are the average of two independent experiments with associated error bars. k_{obs1} exhibits a linear concentration dependence that when fitted to eq 6 (see Materials and Methods) yields a value for the bimolecular rate constant, k_1, of 1.24 ($\pm$ 0.01) $\times$ 10^6 M^{-1} s^{-1} and a value for k_{-1}, obtained from the intercept, of 40 ($\pm$ 2) s^{-1}.

determined the individual association and dissociation rate constants for the E9 DNase−Im9 complex in the presence and absence of bound Zn^{2+}. Values of k_1 (9×10^7 M^{-1} s^{-1}) and k_{off} (1.9×10^{-6} s^{-1}) in pH 7 buffer containing 200 mM NaCl and at 25 °C were essentially identical with or without bound metal ion indicating that the bound metal ion does not affect the kinetics or thermodynamics of immunity protein binding (data not shown). Hence, conformational changes induced by metal ion binding are also independent of Im9 binding. This latter observation has important consequences for the mechanism of cell entry by colicin E9 proposed by Pommer et al. (*20*). The removal of bound metal ion was proposed to destablize the high affinity colicin DNase−immunity protein complex (K_d, 10^{-14} M; ref *22*), accelerating the dissociation rate constant so that it is not rate-limiting for toxin-induced cell death. Since the present experiments discount this possibility, some other factor must be involved in enhancing the dissociation of the colicin−immunity protein complex at the cell surface.

Dissociation of Metal Ions Occurs by a Multistep Process. The dissociation rate constant (k_{off}) was measured by mixing a preformed E9 DNase−metal ion complex with EDTA in a stopped-flow experiment to compare the kinetically derived equilibrium constant ($K_d = k_{off}/k_1$) with previous values of K_d determined by isothermal titration calorimetry (*22*). These experiments can also provide information about the mechanism of binding. We have previously used ANS fluorescence to monitor metal ion binding in static fluorescence experiments (*20*). Upon metal ion binding to the E9 DNase, ANS is excluded from the protein resulting in a decrease in its fluorescence that is reversed by the addition of EDTA (*20*). ANS fluorescence was used to measure the dissociation kinetics in the present work since a greater change in signal is observed compared with the change in tryptophan fluorescence, although with identical results. Since ANS binds to the metal-free E9 DNase within the dead-time of the stopped-flow instrument, and the kinetics of Zn^{2+} binding

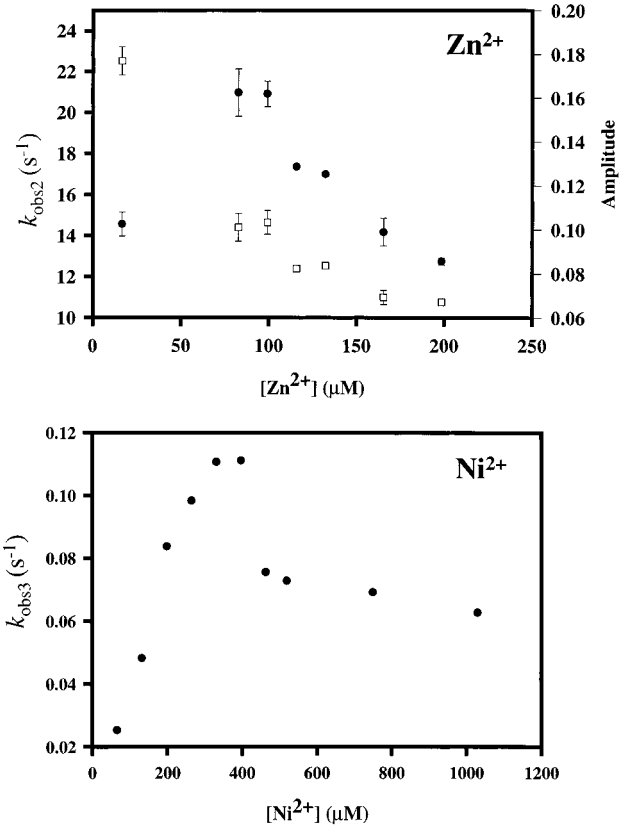

FIGURE 4: Concentration dependence of k_{obs2} (●) and ΔF_{kobs2} (□) for Zn^{2+} binding (top panel) and k_{obs3} for Ni^{2+} binding (lower panel) to 16.5 μM E9 DNase. The first data point for Zn^{2+} data was obtained under second-order conditions using eq 5 (see Materials and Methods) to fit the kinetic trace. All other data points were obtained from experiments carried out under pseudo-first-order conditions where eq 3 was used to fit the kinetic traces. For both metal ions, the observed rate constant forms a skewed bell-shaped curve. The apparent midpoint for the hyperbolic decrease in ΔF_{kobs2} for Zn^{2+} binding is ~70 μM.

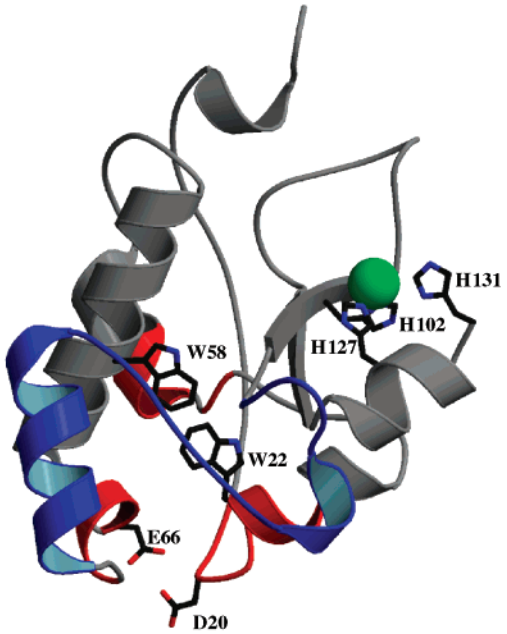

FIGURE 5: Ribbon diagram of the E9 DNase domain showing the Im9 binding site (labeled blue), and the positions of the two buried tryptophans (W22 and W58) relative to the transition metal (green sphere) and the three coordinating histidine residues within the H−N−H motif. Also shown are the two residues (D20 and E66) that were substituted for cysteine to generate an intramolecular disulfide bond across conformationally mobile regions of the DNase (labeled red) (*21*, *27*).

Scheme 2

$$E + M \underset{k_{-1}}{\rightleftharpoons} EM^{a} \underset{k_{-2}}{\rightleftharpoons} EM^{b} \underset{k_{-3}}{\rightleftharpoons} EM^{c} \underset{k_{-4}}{\rightleftharpoons} EM^{d}$$

monitored using ANS fluorescence are essentially identical to those described above (data not shown), metal ion dissociation rather than ANS rebinding is being monitored in these experiments.

Figure 7 shows that Zn^{2+} dissociation is complex and occurs minimally by a four-step process, demonstrating the presence of an additional step in the binding mechanism of Zn^{2+} to the E9 DNase. Although Ni^{2+} dissociation was too slow to be accurately measured by this method ($<10^{-3}$ s^{-1}), multistep dissociation kinetics were observed for Co^{2+} and Cu^{2+} (data not shown), suggesting that it is a common feature of metal ion dissociation from the E9 DNase. Since the observed rate constants (and number of observed steps) are metal ion dependent (Table 1) it implies that the multiple phases in the dissociation experiments are not due to EDTA effects. Multiple dissociation phases with similar rate constants were also seen in the presence of 1 M NaCl, indicating that they are not due to the electrostatic association of the chelating agent with the enzyme (data not shown).

If a ligand binds in a four-step sequential mechanism, such as that depicted in Scheme 2, the expectation is that a single step (k_{-4}) should be rate-limiting for dissociation. The observation that metal ion dissociation occurs in multiple steps for the E9 DNase−Zn^{2+} complex (Figure 7) is however inconsistent with such a mechanism, and instead implies that the metal ion is distributed between different enzyme conformers (such as depicted in Scheme 3) each with a different fluorescence intensity. In such a case, different routes of metal ion dissociation occur from the different enzyme conformers. Therefore, the metal bound state of the

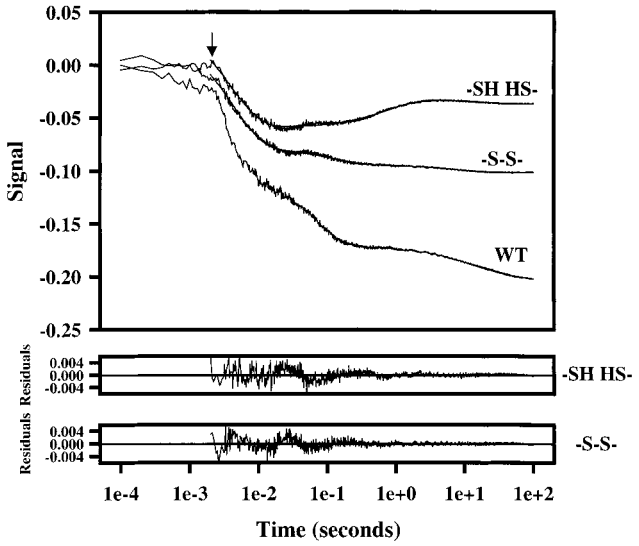

FIGURE 6: Stopped-flow tryptophan fluorescence data showing Zn^{2+} binding to E9 DNase D20C/E66C double mutant (top panel), conditions as described in the legend to Figure 1. Binding to wild-type protein is shown for comparison. Multistep metal binding kinetics are observed regardless of whether an intramolecular disulfide bond is formed, although the amplitudes of the phases differ between the different proteins. The data were fitted to triple exponential equations for the oxidized (-S−S-) mutant to produce $k_{obs1} = 232$ s^{-1} ($\Delta F_{kobs1} = 0.11$), $k_{obs2} = 7.7$ s^{-1} ($\Delta F_{kobs2} = 0.016$), and $k_{obs3} = 0.13$ s^{-1} ($\Delta F_{kobs3} = 0.007$), and the reduced (-SH HS-) mutant to produce $k_{obs1} = 248.2$ s^{-1} ($\Delta F_{kobs1} = 0.105$), $k_{obs2} = 1.26$ s^{-1} ($\Delta F_{kobs2} = -0.027$), and $k_{obs3} = 0.055$ s^{-1} ($\Delta F_{kobs3} = 0.004$) with the fits overlaid on the data. The start of the fitted data (2 ms) is indicated with an arrow. Lower panels show residuals to the fitted data. Although a pattern is observed in the residuals, this is very small relative to the total amplitude change.

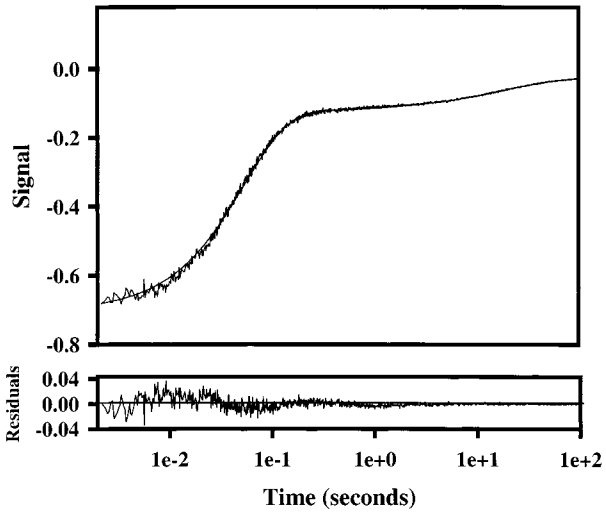

FIGURE 7: Dissociation of Zn^{2+} from the E9 DNase (13.2 μM) using EDTA (20 μM) monitored by stopped-flow ANS fluorescence (top panel). Conditions as described in Materials and Methods. Data were fitted to a quadruple exponential equation to produce $k_{obs1} = 18.45$ s^{-1} ($\Delta F_{kobs1} = 0.579$), $k_{obs2} = 0.63s^{-1}$ ($\Delta F_{kobs2} = 0.011$), $k_{obs3} = 0.063$ s^{-1} ($\Delta F_{kobs3} = 0.067$), $k_{obs4} = 0.0077$ s^{-1} ($\Delta F_{kobs2} = 0.035$). The fit has been overlaid onto the data with the residuals to the fit shown in the lower panel. Mixing EDTA with metal-free E9 DNase produces no fluorescence changes (data not shown).

E9 DNase likely reflects a mixed population of complexes. A similar mechanism has been proposed to explain the multistep dissociation of Mn^{2+} from FosA (*30*).

The importance of (at least one) of the conformational change states to metal binding is highlighted by the

Scheme 3

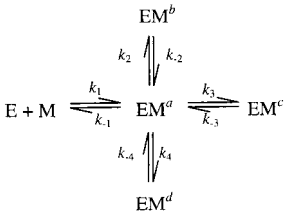

Table 2: Comparison of Kinetically Derived and Equilibrium Measurements of K_d for E9 DNase−Metal Complexes.

metal	K_d (M) [a]	K_d (M) (this work)
Co^{2+}	1.8×10^{-6}	0.99×10^{-6} [b]
		2.3×10^{-6} [c]
Ni^{2+}	0.7×10^{-6}	$\sim 10^{-7}$
Cu^{2+}	n.d.[e]	0.33×10^{-6}
Zn^{2+}	$\sim 3 \times 10^{-9}$	6.2×10^{-9} [b]
		3.6×10^{-9} [d]

[a] Values previously determined by isothermal titration calorimetry (*20*). [b] Value obtained from $K_d = k_{off}/k_1$. [c,d] Values obtained by taking into account the observed microscopic rate constants. [c] $K_d = k_{-1}k_{-2}/k_1k_2$. [d] $K_d = k_{-1}k_{-2}k_{-3}k_{-4}/k_1k_2k_3k_4$ (see Table 3 and the text). [e] n.d., not determined.

magnitude of the equilibrium dissociation constant for the first (bimolecular) step (~30 μM) for Zn^{2+} binding to the E9 DNase. This is four-orders of magnitude weaker than that of the final complex (~3 nM), implying that the structural readjustment(s) result in the formation of a high affinity complex.

Given the presence of multiple complexes depicted in Scheme 3, it is not immediately obvious which observed dissociation rate constant (k_{-n}) should be rate-determining for the overall rate of dissociation, k_{off}. The first observed rate constant for Zn^{2+} dissociation (k_{obs1}) in Figure 7 produces the largest amplitude change (~84%), and the same was seen in tryptophan fluorescence experiments. The first step is also the major phase in Co^{2+} and Cu^{2+} dissociation (data not shown). Initially, this appears to indicate that k_{obs1} defines metal ion binding and so is a good candidate for the step that limits k_{off}, the overall rate of metal ion dissociation. However, k_{obs1} in these EDTA chase experiments has a value of 18.5 s^{-1}, close to the value for k_{-1} determined from the Zn^{2+} association experiments (40 s^{-1}), and would yield a calculated K_d (k_{-1}/k_1) for the E9 DNase−Zn^{2+} complex of 15 μM implying that k_{obs1} is unlikely to be rate-determining for k_{off}. A similar conclusion can be drawn for the kinetics of Co^{2+} binding. Instead, k_{obs4} (0.0077 s^{-1}), the slowest rate in the dissociation experiments with a relatively small amplitude change (Figure 7), is most likely rate-determining for k_{off} for Zn^{2+} since it results in a K_d value of 6.2 nM, close to the K_d obtained by equilibrium methods (Table 2) (*20*).

Single Tryptophan E9 DNase Phenylalanine Mutants as Probes of Mechanism. The E9 DNase contains two tryptophans (W22 and W58; Figure 5) that are 15 and 13 Å, respectively, from the transition metal binding site, but <5 Å from each other and so close enough for energy transfer to occur (*12*, *41*). To probe the mechanism of metal ion binding to the E9 DNase in the absence of any complicating energy transfer processes, single tryptophan mutants were constructed, W58F (W22+) and W22F (W58+), and the effects of Zn^{2+} and Ni^{2+} binding compared.

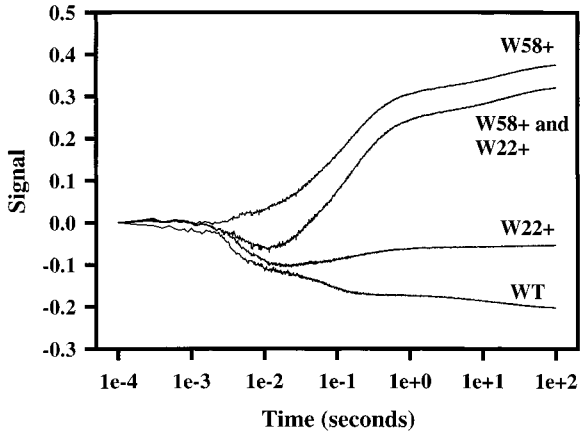

FIGURE 8: Stopped-flow tryptophan fluorescence traces of Zn^{2+} binding to the two single tryptophan mutant E9 DNases, W58+ and W22+. Conditions as described in the legend to Figure 1. Comparison of the W58+ and W22+ traces added together with that of wild-type E9 DNase demonstrates that there is synergy in the fluorescence of the tryptophans in the native protein. Binding of Zn^{2+} to W22+ comprises five transients: $k_{obs1} = 260.1$ s^{-1} ($\Delta F_{kobs1} = 0.068$), which increases linearly with Zn^{2+} concentration, $k_{obs2} = 7$ s^{-1} ($\Delta F_{kobs2} = -0.025$), $k_{obs3} = 2.5$ s^{-1} ($\Delta F_{kobs3} = -0.015$), $k_{obs4} = 0.5$ s^{-1} ($\Delta F_{kobs4} = -0.005$), $k_{obs5} = 0.05$ s^{-1} ($\Delta F_{kobs5} = -0.006$) with the additional rate constants showing no appreciable concentration dependence. Binding to W58+ comprises three transients: $k_{obs1} = 19$ s^{-1} ($\Delta F_{kobs1} = -0.10$), which increases hyperbolically with Zn^{2+} concentration (data not shown), $k_{obs2} = 2.5$ s^{-1} ($\Delta F_{kobs2} = -0.09$), $k_{obs3} = 0.06$ s^{-1} ($\Delta F_{kobs2} = -0.06$), with the additional rate constants showing no appreciable concentration dependence.

Static fluorescence measurements of W22+ ($\lambda^{em}_{max} = 328$ nm) and W58+ ($\lambda^{em}_{max} = 338$ nm) E9 DNases suggest that both are folded (λ^{em}_{max} wild type = 333 nm). Both bind transition metals with 1:1 stoichiometry, and both are active in DNase activity assays (data not shown). Stopped-flow tryptophan fluorescence data were collected for the single tryptophan mutants binding Zn^{2+} and Ni^{2+}, with the data for Zn^{2+} presented in Figure 8. A comparison with the trace for wild-type E9 DNase binding Zn^{2+} indicates that the two mutants differ significantly both from each other and from the wild-type protein, with similar differences evident for Ni^{2+} binding (data not shown). This implies that there is a synergistic change in the fluorescence of the two tryptophans as a result of energy transfer between them in the wild-type E9 DNase. Figure 8 also shows that the two tryptophans are not monitoring metal binding in the same way, although both signal multistep Zn^{2+} binding kinetics, with between three and five transients resolved some with comparatively small amplitude changes (Table 3). It is noteworthy that none of the observed rate constants (for either metal) have the unusual concentration dependences seen in the wild-type enzyme, emphasizing the importance of deconvoluting the metal-binding mechanism through the use of single tryptophan mutants (Figure 4).

Analysis of the tryptophan mutants also shows that detection of the Zn^{2+} bimolecular step is dominated by W22+ since k^{W22+}_{obs1} has a linear concentration dependence similar to the wild-type protein (Table 3). Conversely, W58 largely monitors a conformational change after the bimolecular step since k^{W58+}_{obs1} has a positive hyperbolic concentration dependence (which plateaus at ~40 s^{-1}). ΔF^{W58+}_{kobs1} and ΔF^{W58+}_{kobs2} ($k^{W58+}_{obs2} \sim 2.5$ s^{-1} and concentration inde-

Table 3: Summary of Kinetic Data for Ni^{2+} and Zn^{2+} Binding to the W22+ and W58+ Single Tryptophan E9 DNase Mutants[a]

metal	mutant	k_1 ($M^{-1}s^{-1}$)	$k_2 + k_{-2}$ (s^{-1})	$k_3 + k_{-3}$ (s^{-1})	$k_4 + k_{-4}$ (s^{-1})	$k_5 + k_{-5}$ (s^{-1})
Ni^{2+}	W22+	1.5×10^3	~2	n.d.	0.07 (± 0.01)[b]	n.d.
Ni^{2+}	W58+	1.5×10^3[c]	n.d.	0.27 (± 0.01)[c]	0.07 (± 0.01)[b]	n.d.
Zn^{2+}	W22+	1.2 (± 0.05) $\times 10^6$	~9[d]	2.5 (± 0.2)	0.5 (± 0.06)	0.07
Zn^{2+}	W58+	n.d.	40 (± 1)	2.5 (± 0.2)	n.d.	0.07

[a] The numbering of the steps in this table is specific for individual metal ions and highlights how zinc-binding likely has an additional step to that of nickel (see Figure 9 for further details). In light of the branched nature of the mechanism, the numbering of the rate processes is arbitrary and simply listed in order of magnitude. [b] Values at the plateaued (maximal) region of hyperbolic concentration dependence obtained by fitting to eq 7. [c] Values obtained by taking into account rate coupling (*39*). [d] Tentatively assigned as being equivalent although may represent an additional step. n.d., not detected.

pendent) are the two largest amplitude changes for any of the observed conformational change steps in either mutant and therefore are likely to be present (and dominant) in the wild-type protein. Interestingly, ΔF^{W58+}_{kobs1} decreases with increasing Zn^{2+} concentration (data not shown), mirroring the decreasing ΔF^{WT}_{kobs2} (Figure 4). This may account for the apparent decrease in k^{WT}_{obs2} since if ΔF^{W58+}_{kobs1} decreases sufficiently such that ΔF^{W58+}_{kobs2} (concentration-independent) becomes dominant, its rate constant would also become dominant and, since it is slower, the fitted rate constant may appear to decrease. Taking into account the multistep fluorescence changes associated with wild-type enzyme (Figures 1, 4, and 7) and those seen for the single tryptophan mutants (Figure 8) together suggest that Zn^{2+} binding to the E9 DNase involves five observable events (Figure 9 and Table 3).

Ni^{2+} binding to both the W22+ and W58+ DNases results in triphasic fluorescence traces (data not shown), wherein both tryptophans are able to monitor the bimolecular step to give a value close to that of wild type E9 DNase (Table 3). However, only W22+ monitors the 2 s^{-1} concentration-independent conformational change that represents k^{WT}_{obs1} for Ni^{2+} binding. W58+ monitors a conformational change of ~0.3 s^{-1}, and together with W22+ monitors a conformational change of ~0.07 s^{-1}, producing a minimal four-step Ni^{2+} binding mechanism to the E9 DNase (Figure 9).

The rates of some of the conformational changes are similar in both Zn^{2+} and Ni^{2+} binding (Table 3), suggesting some similarities between the mechanisms. Also, the midpoints for observed rate constants that show hyperbolic metal ion concentration dependences are of the order of ~100 μM both in the wild-type E9 DNase and single tryptophan mutants, as well as being observed for both Zn^{2+} and Ni^{2+} binding. Given the likely presence of more than one bound metal ion complex being present in solution, this suggests that some of these concentration dependences are simply monitoring the distribution of the metal ion from one bound complex to another.

One obvious difference in the binding mechanisms of Zn^{2+} and Ni^{2+} is a conformational change step for Zn^{2+} that occurs early in binding but which is absent for Ni^{2+} (the EZ^b complex for Zn^{2+} in Figure 9). Another interesting difference is that although in many instances the observed rate constants for individual steps are similar they are reported by different tryptophans; for example, the rate of formation of EZ^d and EN^d complexes is of the order of 0.3−0.5 s^{-1}, yet this step is reported by Trp22 for Zn^{2+} but Trp58 for Ni^{2+}.

Multistep Binding Is a Generic Feature of Colicin H−N−H Endonucleases. To address whether multistep

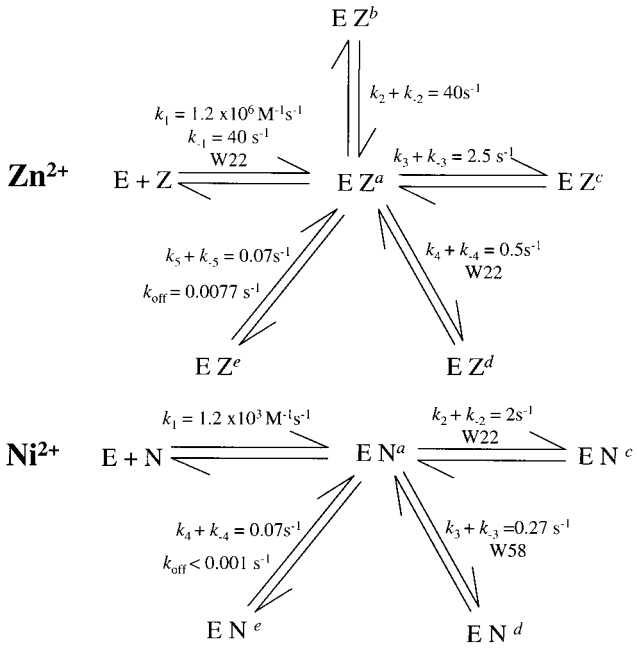

FIGURE 9: Putative kinetic schemes for Zn^{2+} and Ni^{2+} binding to the E9 DNase. Binding of both metal ions to the H−N−H motif of the E9 DNase occurs by a multistep mechanism that produces a metal bound state that is a population of isoforms, indicated by different superscripts (for example, EZ^a is the first intermediate for Zn^{2+} binding). The schemes are consistent with the available kinetic data and have been drawn to illustrate the apparent similarity between Zn^{2+} and Ni^{2+} binding, as evidenced by the similar rate constants describing these processes, and also emphasizes that Zn^{2+} binding includes an additional step (see text for details). In nearly all cases, the quoted values are derived rate constants for individual steps (see Tables 1 and 3), with the exception of k_{off} which represents the slowest observed metal dissociation rate constant obtained by EDTA-sequestration experiments (Figure 7 and Table 1). The assignment of k_{off} to a specific metal-bound isoform is arbitrary. Steps that affect only one of the two DNase tryptophans are identified. No specification is shown where both tryptophans observe the event.

transition metal binding is confined only to the E9 DNase or is a generic feature of all colicin H−N−H endonucleases, Zn^{2+} binding to the E2, E7, and E8 DNases was carried out by stopped-flow fluorescence (Figure 10). Multiple phases were seen for all colicin DNases, showing that this is a conserved feature in this family of proteins. However, the stopped-flow traces were different to the E9 DNase despite W22 and W58 being conserved. The E2, E8, E9 DNases all show quenches upon Zn^{2+} binding with a fast first step, although this appears to be absent from E7 which instead yields an enhancement, reminiscent of the W58+ mutant with the λ_{max} also being similar (338 nm). This suggests that

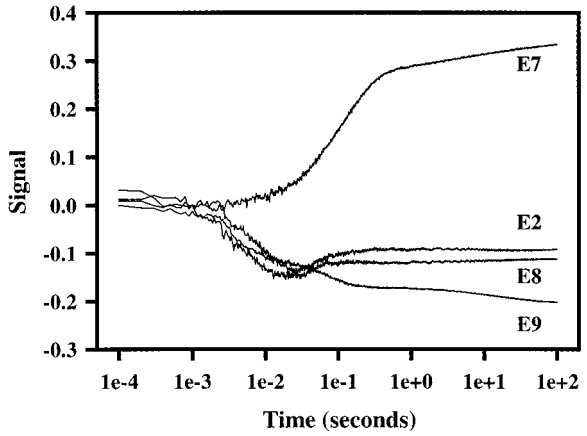

FIGURE 10: Stopped flow tryptophan fluorescence traces demonstrating that multiple transients are observed when Zn^{2+} binds to each of the colicin H−N−H endonucleases E2, E7, E8, and E9. Conditions as described in the legend to Figure 1.

although multistep metal binding is conserved among H−N−H enzymes their mechanistic details differ, possibly as a result of amino acid variations around the two tryptophans.

Relating Colicin DNase Structures to the Kinetics of Metal Binding. The kinetically derived binding affinities for the different metal ions (Table 2) show reasonable agreement with those determined by equilibrium methods, and also show for the first time that Cu^{2+} (an active metal ion) binds with micromolar affinity, similar to that of other "active" metal ions, Ni^{2+} and Co^{2+}. In addition, the kinetic analysis, focusing on a comparison of Zn^{2+} and Ni^{2+} binding to wild type and mutant DNases, has identified mechanistic similarities as well as differences between these metals. Binding for both is best described by a branched, conformational change mechanism in which the complex following the initial bimolecular collision can take one of several paths, many of which appear to share similar rate constants (Figure 9) and involving protein−metal conformers that likely interconvert with one another. In the following analysis, we draw attention to the structural similarities and differences between Zn^{2+}- and Ni^{2+}-bound DNases and attempt to link these to their kinetic mechanisms and to their differing abilities to endow the enzyme with catalytic activity.

In trying to rationalize why zinc is inactive in the H−N−H motif whereas other first row transition metals such as Ni^{2+} and Co^{2+} are active, Pommer et al (*11*) pointed out that Zn^{2+} binds 3-orders of magnitude more tightly than Ni^{2+} or Co^{2+} and suggested that this was the basis for the lack of enzymatic activity. The differences in binding affinity stems from subtle differences in metal ligation in the H−N−H motif, as defined by crystallography, in which Zn^{2+} has three clearly identifiable histidine ligands compared to two for Ni^{2+} (*12*, *13*). This difference is important for catalytic activity since transition metal-mediated cleavage of DNA by colicin DNases likely requires two free coordination sites, one for the scissile phosphodiester oxygen and one for an activated water molecule (*11*).

A comparison of the Ni^{2+}-liganded E9 DNase crystal structure with that of the Zn^{2+}-liganded E7 DNase indicates that there are few other differences between the side-chains surrounding the metal ions. This is in contrast to the structure of the apo-E9 DNase (*19*) wherein the positions of several H−N−H amino acids are altered, and this is consistent with the present kinetic data that resolve several metal-induced conformational changes. Since the structural rearrangements accompanying metal binding appear localized to the H−N−H motif, this implies that it is these conformational changes that are communicated to the buried tryptophans of the E9 DNase even though they are >13 Å from the metal ion.

Pommer et al (*11*) have postulated that H−N−H enzymes exhibit two distinct catalytic mechanisms, one that is Mg^{2+}-dependent, preferentially cleaving double-stranded DNA, the other transition-metal dependent, preferentially cleaving single-stranded DNA. Although Mg^{2+} does not bind directly to the enzyme, it is thought that it associates in the context of bound DNA (*11*, *20*). Moreover, it has been suggested that the crystal structure of the apo-E9 DNase represents that which is poised for Mg^{2+}-dependent catalysis (*11*). The H−N−H motif in this form of the enzyme contains a central salt bridge between E100 and R96 to which are hydrogen bonded two essential histidine residues, H102 and H127, respectively. Binding of transition metals leaves the E100−R96 salt bridge intact but disrupts the hydrogen bonds to the histidine residues which now become co-opted as metal ligands, with bond distances of ∼2.1 Å (Figure 5). The structural similarities between Zn^{2+}- and Ni^{2+}-bound colicin DNases explains the similarities in their kinetic binding mechanisms since they cause similar side-chain rearrangements within the H−N−H motif.

The only clear coordination differences for Zn^{2+} and Ni^{2+}-bound enzymes concern the third and fourth ligation positions. In zinc-bound E7 DNase, these are taken by H131 (2.6 Å) and a bound water molecule (*13*), whereas the X-ray structure of the nickel-bound E9 DNase a phosphate molecule takes the third coordination site with H131 too distant to be a clear fourth metal ligand (∼3.8 Å) (*12*). Since phosphate was omitted from the kinetic experiments, we assume that a water molecule takes the fourth coordination site in the current work. Certainly the only amino acid ligation difference between Zn^{2+} and Ni^{2+} bound DNases is the H131−metal bond distance which is ∼1.2 Å longer in the case of Ni^{2+} than Zn^{2+}. This small difference nevertheless appears to have a profound effect on the affinity of the E9 DNase for metals since alanine mutants of both H102 and H127 reduce Zn^{2+} binding by $\sim 10^6$-fold, whereas a H131A mutant reduces Zn^{2+} binding by only $\sim 10^3$-fold (Walker, Kleanthous & James, unpublished results). We speculate that the extra step that is evident in the kinetic mechanism of Zn^{2+} binding to the E9 DNase relative to Ni^{2+} (Figure 9) involves the movement of H131 to coordinate the metal ion. In the case of Zn^{2+}, this results in a high affinity complex, along with H102 and H127, which inactivates the enzyme due to the availability of only one free coordination site for catalysis. Whereas when Ni^{2+} (and presumably, Co^{2+} and Cu^{2+}) binds, H131 can only form a weak (long-bond) interaction that does not fully occupy a coordination site and so endows the enzyme with catalytic activity.

CONCLUSIONS

Transition metal binding to the H−N−H/treble-clef zinc finger motif of the E9 DNase occurs through a branched, multistep, conformational change mechanism to produce a range of interconverting protein−metal complexes. The

kinetically derived K_d values for Ni^{2+}, Co^{2+}, and Zn^{2+} are in close agreement with those determined previously by titration calorimetry (*20*) arguing that the kinetic mechanisms presented here are a reasonable description of metal binding to the H−N−H motif. All colicin DNases display multistep binding kinetics showing that this is a conserved feature of colicin and most likely all H−N−H endonucleases. The use of single tryptophan-to-phenylalanine mutants has helped resolve the binding mechanisms of Ni^{2+} and Zn^{2+} to the E9 DNase and specifically shown that there is an additional step for Zn^{2+} binding that is absent for Ni^{2+}. This additional step appears linked to the subtle repositioning of a critical histidine residue in the H−N−H motif which forms a stronger interaction with Zn^{2+} than Ni^{2+}, the result of which is to render the enzyme catalytically inactive for the tighter binding metal ion.

ACKNOWLEDGMENT

We would like to thank Andrew Leech, Theonie Georgiou, Daniel Walker, and the members of the Colicin Research Group for valuable discussions, and Christine Moore for technical assistance with the protein purifications. We are also grateful to the referees of this paper for their helpful comments on the kinetic analysis.

REFERENCES

1. Venter, C. J., Adams, M. D., and Myers, E. W., et al. (2001) *Science 291*, 1304−1351.
2. James, R., Kleanthous, C., and Moore, G. R. (1996) *Microbiology 142*, 1569−1580.
3. Gorbalenya A. E. (1994) *Protein Sci. 3*, 1117−1120.
4. Shub, D. A., Goodrich-Blair, H., and Eddy, S. R. (1994) *Trends Biochem. Sci. 19*, 402−404.
5. Belfort, M., and Roberts R. J. (1997) *Nucleic Acids Res. 25*, 3379−3388.
6. Chevalier, B. S., and Stoddard, B. L. (2001) *Nucleic Acid. Res. 29*, 3757−3774.
7. Dalgaard, J. Z., Klar, A. J., Moser, M. J., Holley, W. R., Chatterjee, A., and Mian, I. S. (1997) *Nucleic Acids Res. 25*, 4626−4638.
8. Malik H. S., and Henikoff S. (2000) *Trends Biochem Sci. 25*, 414−418.
9. Aravind, L., Makarova, K. S., and Koonin, E. V. (2000) *Nucleic Acids Res. 28*, 3417−3432.
10. Bujnicki, J. M., Radlinska, M., and Rychlewski, L. (2001) *Trends Biochem. Sci. 26*, 9−11.
11. Pommer, A. J., Cal, S., Keeble, A. H., Walker, D., Evans, S. J., Kühlmann, U. C., Cooper, A., Connolly, B. A., Hemmings, A. M., Moore, G. R., James, R., and Kleanthous, C. (2001) *J. Mol. Biol. 314*, 735−749.
12. Kleanthous, C., Kühlmann, U. C., Pommer, A. J., Ferguson, N., Radford, S. E., Moore, G. R., James, R., and Hemmings, A. M. (1999) *Nat. Struct. Biol. 6*, 243−252.
13. Ko, T.P., Liao, C. C., Ku, W. Y., Chak, K. F., and Yuan, H. S. (1999) *Structure 7*, 91−102.
14. Hannan, J. P., Whittaker, S. B.-M., Hemmings, A. M., James, R., Kleanthous, C., and Moore, G. R. (2000) *J. Inorg. Biochem. 8*, 1711−1713.
15. Garinot-Schneider, C., Pommer, A. J., Moore, G. R., Kleanthous, C., and James, R. (1996). *J. Mol. Biol. 260*, 731−742.
16. Kühlmann, U. C., Moore, G. R., James, R., Kleanthous, C., and Hemmings, A. M. (1999) *FEBS Lett. 463*, 1−2.
17. Grishin, N. V. (2001) *Nucleic Acids Res. 29*, 1703−1714.
18. Laity, J. H., Lee, B. M., and Wright, P. E. (2001) *Curr. Opin. Struct. Biol. 11*, 39−46.
19. Kühlmann, U. C., Pommer, A. J., Moore, G. R., James, R., and Kleanthous, C. (2000) *J.* Mol. Biol. *301*, 1163−1178.
20. Pommer, A. J., Kühlmann, U. C., Cooper, A., Hemmings, A. M., Moore, G. R., James, R., and Kleanthous, C. (1999) *J Biol Chem. 274*, 27153−27160.
21. Whittaker, S. B.-M., Boetzel, R., MacDonald, C., Lian, L.-Y., Pommer, A. J., Reilly, A., James, R., Kleanthous, C. and Moore, G. R. (1998) *J. Biomol. NMR 12*, 145−159.
22. Wallis, R., Moore, G. R., James, R., and Kleanthous, C. (1995) *Biochemistry*, *34*, 13743−13750.
23. Pommer, A. J., Wallis, R., Moore, G. R., James, R., and Kleanthous, C. (1998). *Biochem J. 334*, 387−392.
24. Lazdunski, C. J., Bouveret, E., Rigal, A., Journet, L., Lloubes, R., and Benedetti, H. (1998) *J. Bacteriol. 180*, 4993−5002.
25. Kleanthous, C., Hemmings, A. M., Moore, G. R., and James, R. (1998) *Mol. Microbiol. 28*, 227−233.
26. Kleanthous, C., and Walker, D (2001) *Trends Biochem. Sci. 26*, 624−631.
27. Mosbahi, K., Lemaître, C., Keeble, A. H., Mobasheri, H., Morel, B., James, R., Moore, G. R., Lea, E. J. A., and Kleanthous, C. (2002) *Nature Struct. Biol. 9*, 476−484.
28. Walmsley, A. R., and Bagshaw, C. R. (1989) *Anal. Biochem. 176*, 313−318.
29. Hiromi, K. (1979) *Kinetics of Fast Enzyme Reactions*, John Wiley & Sons, Haltsted Press, New York.
30. Bernat, B. A., and Armstrong, R. N. (2001) *Biochemistry 40*, 12712−12718.
31. Kiefer, L. L., Paterno, S. A., and Fierke, C. A. (1995) *J. Am. Chem. Soc. 117*, 6831−6837.
32. Dawson, R. M. C., Elliott, D. C., Elliott, W. H., and Jones, K. M. (1986) *Data for Biochemical Research*, 3rd ed., Clarendon Press, Oxford.
33. Gutfreund, H. (1995). *Kinetics for the Life Sciences*, Cambridge University Press, Cambridge.
34. Bagshaw, C. R., Eccleston, J. F., Eckstein, F., Goody, R. S., Gutfreund, H., and Trentham, D. R. (1974) *Biochem. J. 141*, 351−364.
35. Ku, W.-Y., Liu, Y.-W., Hsu, Y.-C., Liao, C.-C., Liang, P.-H., Yuan, H. S., and Chak, K−F. (2002) *Nucleic Acid Res. 30*, 1670−1678.
36. Eigen, M., and Hammes, G. G. (1963) *Adv. Enzymol. 25*, 1−38.
37. Henkens, R. W., and Strutevant, J. M. (1968) *J. Am. Chem. Soc. 90*, 2669−2676.
38. Kirschner, K., Eigen, M., Bittman, R., and Voigt, B. (1966) *Proc. Natl. Acad. Sci. 56*, 1661−1667.
39. Bernasconi, C. F. (1976) *Relaxation Kinetics*, Academic Press, New York.
40. Hannan, J. P., Whittaker, S. B., Hemmings, A. M., James, R., Kleanthous, C., and Moore, G. R. (2000) *J. Inorg. Biochem. 79*, 365−370.
41. Lakowicz, J. R. (1999) *Principles of Fluorescence Spectroscopy*, 2nd ed., Kluwer Academic/Plenum Publishers, New York, USA.

BI020174O